Accurate BDD-based Unitary Operator Manipulation for Scalable and Robust Quantum Circuit Verification

Chun-Yu Wei[†], Yuan-Hung Tsai[†], Chiao-Shan Jhang[‡], and Jie-Hong R. Jiang[†‡]
[†]Graduate Institute of Electronics Engineering, National Taiwan University, Taipei, Taiwan
[‡]Department of Electrical Engineering, National Taiwan University, Taipei, Taiwan

ABSTRACT

Quantum circuit verification is essential, ensuring that quantum program compilation yields a sequence of primitive unitary operators executable correctly and reliably on a quantum processor. Most prior quantum circuit equivalence checking methods rely on edge-weighted decision diagrams and suffer from scalability and verification accuracy issues. This work overcomes these issues by extending a recent BDD-based algebraic representation of state vectors to support unitary operator manipulation. Experimental results demonstrate the superiority of the new method in scalability and exactness in contrast to the inexactness of prior approaches. Also, our method is much more robust in verifying dissimilar circuits than previous work.

1 INTRODUCTION

The rapid progress of quantum technologies has opened the door to the noisy intermediate-scale quantum (NISQ) era. More and more applications are identified to benefit from taking advantage of quantum computation. Also, software tools, e.g., [1, 4], are actively developed making quantum computation accessible. Among them, simulation and verification tools are essential elements to assist quantum program development. In this work, we are concerned with quantum circuit verification, mainly equivalence checking.

Many solutions have also been proposed for the equivalence checking of quantum circuits, e.g, re-writing [17], Boolean satisfiability (SAT) [16], and decision diagram (DD) based methods [3, 7]. However, re-writing methods can be limited when structurally dissimilar circuits are to be verified. SAT-based methods suffer from the formula explosion problem to encode infinite-valued quantum states. DD-based methods [3, 7] provide a canonical and compact representation for quantum circuit manipulation. While this canonicity eases equivalence checking, it inevitably incurs the well-known memory blowup problem. The state-of-the-art method [3] is based on the Quantum Multiple-valued Decision Diagram (QMDD) [11, 18]. The data structure consists of decision nodes with four-valued branching for matrix representation and edges weighted with complex numbers stored in the floating point data type. It suffers from the precision loss problem, which may result in incorrect verification answers. In [7], equivalence checking of noisy quantum circuits is studied using Tensor Decision Diagram (TDD) [8], a variant of QMDD.

DAC '22, July 10–14, 2022, San Francisco, CA, USA
© 2022 Association for Computing Machinery.
ACM ISBN 978-1-4503-9142-9/22/07…$15.00
https://doi.org/10.1145/3489517.3530481

The main results of this work are as follows. First, we overcome the precision loss problem and alleviate the memory blowup issue by extending the recent binary decision diagram (BDD) based algebraic representation of quantum states [14] to quantum unitary operators. This representation allows exact manipulation (multiplication) of the considered universal set of unitary operators. Thereby the equivalence checking, unlike prior work, is made exact without the precision problem. Second, we generalize the decision problem of equivalence checking to a quantitative verification problem by using fidelity (with value between 0 and 1) as a metric to assess the (dis)similarity between two quantum circuits under checking. When the fidelity value equals 1, it indicates two circuits under checking are equivalent. Otherwise, it indicates the two circuits are nonequivalent. Further, the smaller the fidelity value, the larger the dissimilarity between the circuits. Third, the scalability, accuracy, and robustness of our method are demonstrated through a set of experiments compared to the state-of-the-art methods.

2 PRELIMINARIES

As a notational convention, we denote variables with lower-case letters, e.g., x, Boolean functions and their BDDs with upper-case letters, e.g., F. For Boolean connectives, we denote negation by overline or $\neg$, conjunction by $\wedge$, and disjunction by $\vee$. For simplicity, we sometimes omit $\wedge$ in a formula. We refer to a *literal* as a Boolean variable or the negation of a variable.

2.1 Quantum State Representation and Evolution

The state of an n-qubit quantum system is represented by a $2^n \times 1$ vector of complex numbers and the state evolution can be described by the transformation of a $2^n \times 2^n$ unitary matrix. A matrix U is unitary if its inverse U^{-1} equals its conjugate transpose $U^{\dagger}$. A quantum circuit consists of a set of quantum gates, also referred to as unitary operators, say $U_1, \ldots, U_m$ in order. Let $|\psi_0\rangle$ be the initial input state and $|\psi_m\rangle$ be the final output state of the circuit. Then

$$|\psi_m\rangle = U_m \times U_{m-1} \times \cdots \times U_1 \times |\psi_0\rangle . \quad (1)$$

Note that the product of two unitary matrices remains unitary.

In [19], an algebraic representation of complex numbers is proposed. Specifically, a complex number $\alpha \in \mathbb{C}$ is expressed by

$$\alpha = \frac{1}{\sqrt{2}^k}(a\omega^3 + b\omega^2 + c\omega + d), \quad (2)$$

where the coefficients $a, b, c, d, k \in \mathbb{Z}$, and $\omega = e^{\imath\pi/4}$. By Eq. (2), a $2^n \times 1$ state vector is expressed by an integer scalar k and four vectors $\vec{a} = [a_0, \ldots, a_{2^n-1}]^T, \vec{b} = [b_0, \ldots, b_{2^n-1}]^T, \vec{c} = [c_0, \ldots, c_{2^n-1}]^T, \vec{d} =$

$[d_0, \ldots, d_{2^n-1}]^T$, each with 2^n entries of integer values. In [14], the four integer vectors are represented by BDDs in a bit-sliced manner. For integers in the r-bit 2's complement form (r dynamically adjustable), each of $\vec{a}, \vec{b}, \vec{c}, \vec{d}$ is expressed with r BDDs of n variables. That is, each bit, say the i^{th} bit, of $\vec{a}$ (similarly, $\vec{b}, \vec{c}, \vec{d}$), i.e., the bit-vector $[a_{0,i}, \ldots, a_{2^n-1,i}]^T$, is treated as the truth table of an n-variable function and represented by an n-variable BDD. On the other hand, as scalar k is shared among all 2^n entries of $\vec{a}, \vec{b}, \vec{c}, \vec{d}$, it is stored separately. Overall $4r$ BDDs over n variables are used to represent an n-qubit state vector. In the sequel, the BDDs of the i^{th} bit of $\vec{a}$, $\vec{b}$, $\vec{c}$, and $\vec{d}$ are referred to as F^{ai}, F^{bi}, F^{ci}, and F^{di}, respectively.

Furthermore, to support state evolution computation, a state vector has to be multiplied with a unitary operator. The quantum gate set supported in [14] includes $\{X, Y, Z, H, S, T, R_x(\pi/2), R_y(\pi/2)$, CNOT, CZ, multi-control Toffoli, multi-control Fredkin$\}$, which is a superset of a universal quantum gate set able to approximate arbitrary unitary operations. The effects of applying the unitary operators on the current state vector are characterized into Boolean formulas, which can be found in [14], Tables I and II.

In this work, we adopt the algebraic complex number representation and extend the state-vector bit-slicing technique to unitary-matrix bit-slicing. Furthermore, we derive the Boolean formulas characterizing the effects of applying the unitary operators on the current unitary matrix into Boolean formulas.

2.2 Quantum Circuit Equivalence Checking

Given two quantum circuits U and V described in unitary matrices, the quantum circuit equivalence checking problem asks whether $U = e^{\imath\alpha}V$ for some constant $\alpha \in [0, 2\pi)$, i.e., U and V are equivalent up to a global phase factor $e^{\imath\alpha}$, which has no effect on the functionality of a quantum circuit [10]. If so, U and V are *equivalent (EQ)*; otherwise, *nonequivalent (NEQ)*.

A common approach to quantum circuit equivalence checking is to build the miter of two quantum circuits $U = U_{m-1} \cdots U_0$ and $V = V_{p-1} \cdots V_0$ as

$$U \cdot V^{-1} = (U_{m-1} \cdots U_0) \cdot (V_0^{-1} \cdots V_{p-1}^{-1}). \tag{3}$$

Thereby, if the miter $U \cdot V^{-1}$ equals $e^{\imath\alpha}I$, i.e., where I is the identity matrix, then U and V are equivalent.

In [3], Eq. (3) is rewritten as $U_{m-1} \cdots U_0 \cdot I \cdot V_0^{\dagger} \cdots V_{p-1}^{\dagger}$. Initially, let the current matrix be the middle identity matrix I. At each step, the current matrix is multiplied with its left or right adjacent matrix. The process repeats until the current matrix has no more adjacent matrix to multiply. Three multiplication strategies, namely, *naive*, *proportional*, and *look-ahead*, are studied in [3]. In this work, we adopt the *proportional* strategy in our quantum circuit equivalence checking implementation. However, unlike prior work [3] using QMDD, we use bit-sliced BDD-based unitary matrix representation for the computation.

3 UNITARY MATRIX REPRESENTATION AND MANIPULATION

In this section, we extend the BDD-based representation and manipulation [14] for state vectors to unitary matrices.

3.1 Bit-Sliced Representation for Unitary Operators

By Eq. (2), we represent a $2^n \times 2^n$ unitary matrix U algebraically with an integer scalar k and four $2^n \times 2^n$ matrices U^a, U^b, U^c, and U^d with entries of integers. Let an integer be represented as an r-bit 2's complement number. Then the i^{th}-bit values of the $2^n \times 2^n$ integer entries of U^a (similarly, U^b, U^c, U^d) can be represented by a BDD, denoted F^{ai} (similarly, F^{bi}, F^{ci}, F^{di}), of $2n$ variables. Essentially, each qubit requires two variables to indicate the input-output mapping similar to a QMDD. That is, a qubit partitions a unitary matrix U into four submatrices

$$U = \begin{bmatrix} U_{00} & U_{01} \\ U_{10} & U_{11} \end{bmatrix}, \tag{4}$$

where the sub-matrix U_{ij} indicates the mapping of the qubit from the input value $|j\rangle$ to the output value $|i\rangle$ for $i, j \in \{0, 1\}$. For each qubit q, let it be encoded by two Boolean variables q_0 (called the 0-variable of q) and q_1 (the 1-variable), which correspond to the indices i and j in U_{ij}, respectively. Hence, an n-qubit system requires $2n$ variables to address the entries in a $2^n \times 2^n$ matrix.

3.2 Formula Characterization for Matrix Multiplication

Boolean formulas are characterized for applying a unitary operator to the bit-sliced representation of unitary matrix. To take advantage of algebraic representation, we consider multiplying an (algebraically representable) current matrix M with a unitary operator U in $\{X, Y, Z, H, S, T, R_x(\pi/2), R_y(\pi/2)$, CNOT, CZ, multi-control Toffoli, multi-control Fredkin$\}$ [14]. We analyze the cases for multiplication from the left, i.e., $U \cdot M$, and from the right, i.e., $M \cdot U$, as follows. (Recall the matrix multiplication in Section 2.2 is done in two possible directions.)

3.2.1 Multiplication from the Left. Without loss of generality, consider a 2-qubit current matrix

$$M = \begin{bmatrix} \alpha_{0000} & \alpha_{0001} & \alpha_{0100} & \alpha_{0101} \\ \alpha_{0010} & \alpha_{0011} & \alpha_{0110} & \alpha_{0111} \\ \alpha_{1000} & \alpha_{1001} & \alpha_{1100} & \alpha_{1101} \\ \alpha_{1010} & \alpha_{1011} & \alpha_{1110} & \alpha_{1111} \end{bmatrix} \tag{5}$$

where the subscript of entry $\alpha_{p_0 p_1 q_0 q_1}$ corresponds to the values of 0- and 1-variables of qubit p and q. Observe that the entries in the same row have the same values of the 0-variables (colored in red); those in the same column have the same values of the 1-variables. Accordingly, replacing all qubit variables in the formulas in [14] with their 0-variables results in formulas naturally updating each column of the matrix, which is equivalent to multiplying the current matrix with a unitary operator from the left. The above discussion holds for an arbitrary qubit number. Accordingly, for multiplying U from the left of M, the formulas are the same as those in Tables I and II in [14] except that all appearances of qubit variable q_t are replaced with q_{t0}.

3.2.2 Multiplication from the Right. Multiplying the current matrix with a unitary operator from the right is not as natural as that from the left. We analyze the considered set of unitary operators in two cases: the symmetric operators and the asymmetric operators. For the first case, consider symmetric operators, $U \in \{X, Z, H, S, T, R_x(\pi/2)$, CNOT, CZ, multi-control Toffoli, multi-control Fredkin$\}$. For U symmetric, we have $U = U^T$ and thus

$$M \cdot U = (U^T \cdot M^T)^T = (U \cdot M^T)^T. \tag{6}$$

Observe that 1) M^T switches the columns and rows of M, which is equivalent to permuting the corresponding 0-variables and 1-variables in the BDDs representing M, and 2) After U is applied, $(UM^T)^T$ recovers the columns and rows of M. Hence, multiplying M with a symmetric operator U from the right corresponds to replacing all appearances of the qubit variable q_t in its respective formulas in Table I or II in [14] with the 1-variable q_{t1}.

For the second case, consider the asymmetric operators $U \in \{Y, R_y(\pi/2)\}$, which are 1-qubit gates with identical diagonal entries, that is, $\begin{bmatrix} \alpha_{00} & \alpha_{01} \\ \alpha_{10} & \alpha_{11} \end{bmatrix}$ with $\alpha_{01} \neq \alpha_{10}$ and $\alpha_{00} = \alpha_{11}$. When $\alpha_{00} = \alpha_{11}$ and $\alpha_{01} \neq \alpha_{10}$, inverting all qubit variables in the formulas of U effectively results in the formulas of operator $\begin{bmatrix} \alpha_{11} & \alpha_{10} \\ \alpha_{01} & \alpha_{00} \end{bmatrix} = \begin{bmatrix} \alpha_{00} & \alpha_{10} \\ \alpha_{01} & \alpha_{11} \end{bmatrix} = U^T$. Therefore, to obtain the formulas of Y and $R_y(\pi/2)$, in addition to replacing all appearances of the qubit variable q_t in their respective formulas in Tables I and II in [14] with the 1-variable q_{t1} (as done in the first case), we have to further complement every appearance of the qubit variable q_{t1} to implement U^T.

4 QUANTUM CIRCUIT VERIFICATION

This section studies how the bit-sliced BDD-based method for unitary matrix manipulation presented above can be applied to equivalence checking, fidelity checking, and sparsity checking.

4.1 Equivalence Checking

Quantum circuit equivalence checking can be done through the miter construction as mentioned in Section 2.2. The procedure starts from building the current matrix BDDs F^I of the identity matrix. Specifically, all BDDs are initially set to constant 0 (false) except for F^{d0}. Given an n-qubit quantum system, the initial F^{d0} is constructed by

$$F^{d0} = \bigwedge_{j=0}^{n-1} \overline{q_{j0}}\,\overline{q_{j1}} \vee q_{j0}q_{j1} \triangleq F^I, \tag{7}$$

where q_{j0} and q_{j1} are the 0-variable and 1-variable of the formula/BDD under construction corresponding to the j^{th} qubit of the quantum circuit.

The procedure then conducts a sequence of matrix multiplications using the *proportional* strategy mentioned Section 2.2 by applying the formulas of Section 3.2 to update the BDDs of the current matrix. Two circuits U and V are equivalent if the resulting matrix $U \cdot V^{-1}$ realizes $e^{\imath\alpha}I$. In the BDD-based representation, checking if $UV^{-1} = e^{\imath\alpha}I$ is equivalent to checking if the final BDDs correspond to a scalar matrix, i.e., 1) all off-diagonal entries are 0, and 2) all diagonal entries are equal. Under the bit-sliced representation, it is also equivalent to checking if each BDD is either F^I in Eq. (7) or constant 0, thus merely requiring $4r$ BDD pointer comparisons.

4.2 Fidelity Checking

The decision problem of equivalence checking has a yes or no answer, which may not provide much information when the two circuits U and V under checking are nonequivalent. It is sometimes desirable to quantitatively assess how close U and V are. Such quantitative verification can be done through the notion of *fidelity* between two $2^n \times 2^n$ unitary operators U and V defined in [2] by

$$\mathcal{F}(U,V) \triangleq \left| \int_{\psi} \langle \psi | V^{\dagger} U | \psi \rangle \right|^2 = \frac{1}{2^{2n}} \left| \mathrm{tr}\left(UV^{\dagger}\right) \right|^2, \tag{8}$$

which has value ranging from 0 to 1. The larger the value $\mathcal{F}(U,V)$ is, the closer the two circuits U and V are. We refer to computing $\mathcal{F}(U,V)$ as the *fidelity checking*.

Note that after obtaining $UV^{\dagger}$ in equivalence checking, the trace of of the final matrix corresponds to $\mathcal{F}(U,V)$. In fact, the trace can be computed efficiently when the final matrix is represented by QMDD or BDD. In the case of QMDD, the trace can be obtained by traversing only the "00-child" and "11-child" of each node recursively; in the case of our BDD structure, the trace can be obtained similarly by traversing the *combined monolithic BDD* [14]. The "00-child" (resp. "11-child") of a QMDD corresponds to assigning 0 (resp. 1) to both 0- and 1-variables in the BDD counterpart.

Besides the above traversing method, our BDD method allows an even more efficient way without constructing the monolithic BDD, by utilizing the composition operation and the minterm counting algorithm of BDD (both are available in the CUDD package [13]) as follows. Let the BDD composition procedure

$$Compose(F(y, x_1, \ldots, x_m), y, G(x_1, \ldots, x_m))$$

derive the BDD of function $F(G(x_1, \ldots, x_m), x_1, \ldots, x_m)$. Note that, under the bit-sliced matrix representation in Section 3.1, for each diagonal entry of the current matrix M, the 0-variable and 1-variable of a qubit are assigned the same value. Accordingly, we can collect the diagonal entries of M into a $2^n \times 1$ vector by substituting every 1-variable with its corresponding 0-variable. Thus, for each F^{xi}, with $x \in \{a, b, c, d\}$ and $i = 0, \ldots, r-1$ of the $4r$ BDDs of M, we compute $\hat{F}^{xi}$ iteratively, starting from $\hat{F}^{xi} = F^{xi}$, by composing the j^{th} qubit variable q_{j1} with q_{j0} as

$$\hat{F}^{xi} := Compose(\hat{F}^{xi}, q_{j1}, q_{j0}), \tag{9}$$

for $j = 0, \ldots, n-1$. The obtained $4r$ BDDs constitute the desired vectors of $\vec{a}, \vec{b}, \vec{c}, \vec{d}$. The trace of M can be computed by summing up all the 2^n entries for each of the vectors $\vec{a}, \vec{b}, \vec{c}, \vec{d}$. The summations can be done efficiently by minterm counting on each BDD, and then multiplying the result of minterm counting with the corresponding weight of the bit. Recall that the entries of $\vec{a}, \vec{b}, \vec{c}, \vec{d}$ are 2's complement numbers. In this way, we avoid building a monolithic BDD to allow scalable computation.

4.3 Sparsity Checking

As the sparsity (the portion of 0-entries among all entries) of a matrix M is an important factor to certain quantum algorithms, such as the HHL algorithm [6], we study how to compute the sparsity of M under the BDD representation. Observe that in the BDD representation, an entry of M is zero if and only if its corresponding $4r$ BDD values are all zeros. In other words, any non-zero bit makes an entry non-zero. To count the number of zero entries, we can count the number of non-zero entries by first building the disjunction BDD of the $4r$ BDDs and then counting the number of onset minterms on the disjunction BDD. Then, subtracting this number (the number of non-zero entries) from 2^{2n} yields the number of zero entries, and the sparsity can be further calculated.

We note that the sparsity of M represented by QMDD can also be efficiently computed by a single traversal on the QMDD to count the number of "minterms" (full qubit variable assignments) leading to the 0-terminal node, similar to BDD minterm counting.

5 EXPERIMENTAL RESULTS

Our proposed verification method, named `SliQEC`, was implemented in C/C++ and used `CUDD` [13] as the underlying BDD package. The variable reorder option in `CUDD` was turned on by default. The bit length of an integer was set to $r = 32$ by default, and extra bits were allocated when needed. All experiments were conducted on a server with Intel Xeon Silver 4210 CPU at 2.2 GHz and 125 GB RAM. The runtime reported in the experiments is in CPU time measured in seconds (s), while the memory usage is measured in megabytes (MB). The time-out (TO) and memory-out (MO) limits were set to 7200 seconds and 2 GB, respectively.

In the experiments, the state-of-the-art equivalence checker `QCEC` version v1.9.1 [3] (using a default *proportional* strategy), which is based on QMDD and implemented in C++, was compared. Since `QCEC` cannot check fidelity and sparsity, we have implemented them in `QCEC` for comparison with `SliQEC`. The evaluation was performed on four benchmark sets, including Random, Bernstein-Vazirani (BV), Entanglement, and RevLib. The Random benchmark circuits U was randomly generated with Clifford+T and 2-control Toffoli gates, and H gates are applied to all qubits initially to impose superposition. The ratio of the number of gates to the number of qubits was set to 5:1. Ten circuits were generated for each qubit size ranging from 10 to 160. To get circuits V as the counterparts of U for equivalence checking, we replaced all 2-control Toffoli gates in U with a functionally equivalent Clifford+T realization shown in Fig. 1a. To further create circuits nonequivalent to U, one or three gates were randomly removed from V in the experiments. For the BV and Entanglement benchmarks, the U circuits with 60 to 10000 qubits were generated. The V circuits were created by replacing all CNOT gates in U randomly with the three functionally equivalent templates shown in Fig. 1b and 1c [12, 17]. For RevLib benchmarks [15], H gates are applied to all qubits initially to impose superposition as the U circuits. We created the V circuits by rewriting U with the template in Fig. 1a to replace one of the Toffoli gates in U.

5.1 Equivalence and Fidelity Checking

The results on Random benchmarks are shown in Table 1, where Columns 1, 2 and 3 list the number of involved qubits denoted as $\#Q$, the number of gates in U denoted as $\#G$, and the average number of gates in V denoted as $\#G'$. The remaining columns list the average results of runtime and the fidelity denoted as F, for the finished cases. In the table, "error" indicates the number of cases returned with a wrong answer (incorrect EQ or NEQ conclusion). The numbers F (resp. F^-) indicate the fidelity averaged over the cases solved by the underlying method (resp. solved by both `QCEC` and `SliQEC`). As can be seen, `SliQEC` outperformed `QCEC` in for all the EQ and NEQ experiments. For the EQ experiments, `SliQEC` finished all cases without TO and MO. Also, because the fidelity computed by `SliQEC` is exact, the differences in the F^- value between `QCEC`

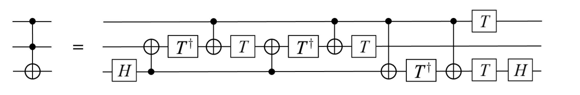

(a) Toffoli.

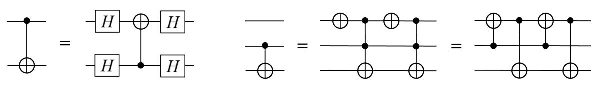

(b) CNOT. (c) CNOT with an ancillary qubit.

Figure 1: Templates for circuit rewriting.

and `SliQEC` indicate the numerical precision loss of `QCEC`. In fact, the precision loss of `QCEC` may result in a wrong answer, e.g., in the 10-qubit EQ experiment. Another trend can be seen by comparing EQ, NEQ 1-gate removal, NEQ 3-gate removal is that increasing the dissimilarities between circuits U and V under checking makes equivalence and fidelity checking harder. Nevertheless, `SliQEC` is more robust than `QCEC` in coping with dissimilar circuits.

The results on BV and Entanglement benchmarks are shown in Table 2. (We omit the results for NEQ experiments as conclusions similar to the EQ experiments can be drawn.) As seen, `SliQEC` outperformed `QCEC` on both benchmarks. For BV circuits with $200 \le \#Q \le 2000$, `QCEC` produced global phases with large amplitudes, possibly due to numerical precision loss, making the fidelity incorrect although it returned correct EQ answers. We also noticed that turning off (indicated "w/o") the BDD reordering option made `SliQEC` perform faster than turning on ("w") for the BV circuits. In general, BDD reordering is helpful but sometimes wasteful.

The results on RevLib benchmarks are shown in Table 3, where only data of cases with more than 100 qubits are reported as small cases can be solved efficiently by both methods. As observed, `SliQEC` outperforms `QCEC`. Also, variable reordering is effective.

5.1.1 Robustness Study. To study the effect of circuit gate count on equivalence checking, we generated 10-qubit random U circuits with the gate counts ranging from 20 to 150, and created the corresponding equivalent V circuits using the Fig. 1a template. For each gate count, 1000 benchmarks were generated. The resultant error rate and average fidelity (y-axis) of `SliQEC` and `QCEC` with respect to the gate count of U (x-axis) were plotted in Fig. 2. (The error rate is the ratio of the number of wrong-answer cases to 1000.) As seen from the plot, `SliQEC` produces correct, exact answers regardless of the gate count increase while the reliability of `QCEC` degrades.

To study the effect of dissimilarity between U and V circuits on equivalence checking, we took small qubit RevLib circuits as U and created very different but equivalent V by repeatedly applying template rewriting using Fig. 1 rules. The results are shown in Table 4. Again, the robustness of `SliQEC` was witnessed.

5.2 Approximate Equivalence Checking on Noisy Quantum Circuits

Approximate equivalence checking of noisy quantum circuits was studied in [7], where TDD [8] was used as the underlying data structure. It relies on the Jamiolkowski fidelity F_J [5] to characterize equivalence. The fidelity F_J between an n-qubit ideal circuit U and

Table 1: Results on Random benchmarks.

#Q	#G	#G'	EQ case						NEQ case (1-gate removal)							NEQ case (3-gate removal)						
			QCEC			SliQEC			QCEC			SliQEC				QCEC			SliQEC			
			Time	F, F^-	TO/MO/error	Time	F	F^-	Time	F, F^-	TO/MO	Time	F	F^-	TO	Time	F, F^-	TO/MO	Time	F	F^-	TO
10	50	169	0.014	0.956	0/0/1	0.048	1	1	0.016	0.249	0/0	0.064	0.260	0.260	0	0.045	0.174	0/0	0.222	0.177	0.177	0
20	100	290.4	0.043	1	0/0/0	0.317	1	1	0.054	0.537	0/0	0.452	0.537	0.537	0	0.106	0.040	0/0	0.732	0.040	0.040	0
30	150	451	0.116	1	0/0/0	1.021	1	1	0.310	0.396	0/0	1.653	0.396	0.396	0	1.188	0.040	0/0	6.429	0.040	0.040	0
40	200	648	1.881	1	0/0/0	2.320	1	1	2.593	0.346	0/0	2.846	0.346	0.346	0	26.499	0.152	0/3	177.637	0.103	0.152	0
50	250	850.6	14.617	1	0/0/0	5.416	1	1	19.541	0.652	0/1	8.986	0.587	0.652	0	25.952	0.182	0/3	450.337	0.149	0.182	1
60	300	979	37.473	1	1/1/0	15.244	1	1	39.282	0.267	1/3	29.464	0.210	0.267	0	128.441	0.094	1/4	45.181	0.052	0.094	0
70	350	1101.8	704.522	1	1/2/0	17.299	1	1	581.067	0.368	1/3	23.790	0.441	0.368	0	637.296	0.311	1/7	124.211	0.110	0.311	1
80	400	1273.6	1203.984	1	3/5/0	27.383	1	1	217.037	0.854	3/6	71.014	0.441	0.854	0	260.115	0.182	3/6	72.383	0.139	0.182	0
90	450	1392.2	200.992	1	5/4/0	26.191	1	1	196.708	0.500	5/4	27.445	0.577	0.500	0	-	-	5/5	236.162	0.054	-	1
100	500	1655	-	-	5/5/0	93.674	1	-	-	-	5/5	104.477	0.441	-	0	-	-	5/5	236.524	0.121	-	1
110	550	1812.8	-	-	9/1/0	72.636	1	-	-	-	9/1	134.408	0.647	-	0	-	-	9/1	259.036	0.085	-	1
120	600	1909	-	-	6/4/0	356.753	1	-	-	-	6/4	125.273	0.423	-	1	-	-	6/4	1362.571	0.167	-	1
130	650	2045.8	-	-	7/3/0	256.338	1	-	-	-	7/3	265.333	0.516	-	0	-	-	7/3	885.882	0.080	-	0
140	700	2259.6	-	-	9/1/0	218.389	1	-	-	-	9/1	437.130	0.260	-	0	-	-	9/1	629.243	0.153	-	2
150	750	2371.2	-	-	10/0/0	386.027	1	-	-	-	10/0	408.942	0.477	-	0	-	-	10/0	542.257	0.031	-	2
160	800	2503.8	-	-	10/0/0	598.274	1	-	-	-	10/0	624.278	0.296	-	0	-	-	10/0	1748.694	0.121	-	2

Table 2: Results on BV and Entanglement benchmarks.

#Q	BV					Entanglement			
	QCEC		SliQEC			QCEC		SliQEC	
	Time	F	Time (w)	Time (w/o)	F	Time	F	Time	F
60	0.078	1	0.306	0.297	1	0.044	1	0.058	1
80	0.146	1	4.314	0.535	1	0.061	1	0.114	1
100	0.283	1	9.653	0.838	1	0.085	1	0.171	1
200	1.963	»1	43.213	4.059	1	0.347	1	23.123	1
400	10.513	»1	407.063	16.403	1	3.197	1	105.148	1
600	30.217	»1	1104.870	33.702	1	11.663	1	172.432	1
800	72.052	»1	281.383	64.551	1	27.780	1	78.843	1
1000	127.119	»1	198.071	98.161	1	55.429	1	50.715	1
2000	332.592	»1	540.796	410.757	1	111.260	1	131.144	1
4000	MO		2136.25	1716.270	1	MO		522.185	1
6000	MO		TO	4074.000	1	MO		1149.520	1
8000	MO		TO	7070.100	1	MO		2051.980	1
10000	MO		TO	TO	-	MO		3405.990	1

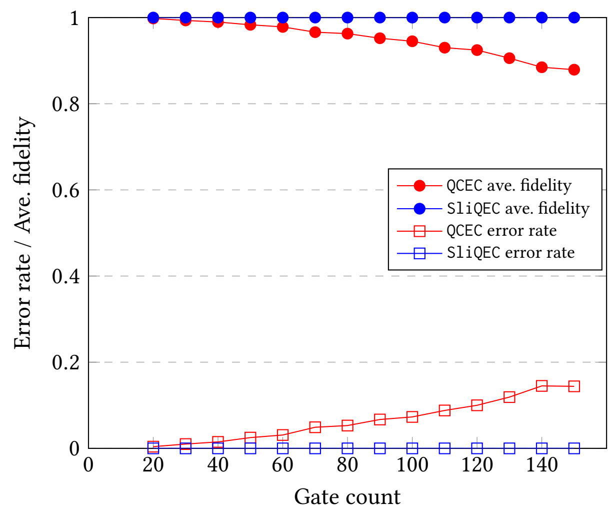

Figure 2: Error rate and fidelity of equivalence checkers in response to gate count increase.

Table 3: Results on RevLib benchmarks.

Benchmarks	#Q	QCEC		SliQEC			
				w reorder		w/o reorder	
		Time	Memory	Time	Memory	Time	Memory
_443	261	MO		TO		MO	
add64_184	193	0.132	121.340	4.197	40.985	0.640	43.725
apex2_289	498	MO		529.028	121.684	278.924	279.249
callif_32_429	130	MO		68.755	95.781	MO	
cps_292	923	MO		1819.730	183.558	976.371	455.827
cpu_control_unit_402	392	MO		197.982	59.089	MO	
ex5p_296	206	6.888	656.843	11.856	44.675	14.221	172.511
hwb9_304	170	15.432	1174.753	17.458	30.298	17.122	163.918
lu_326	299	MO		TO		MO	
nestedif_32_445	263	MO		TO		MO	
pdc_307	619	MO		695.248	84.468	383.118	378.831
spla_315	489	MO		217.719	84.087	111.708	267.272
varpos_32_447	224	MO		36.507	48.501	556.474	1202.823

Table 4: Results on dissimilar RevLib circuits.

Benchmark	#Q	#G	#G'	QCEC		SliQEC	
				Time	Memory	Time	Memory
5xp1_194	17	92	14846	MO		16.655	39.154
add6_196	19	241	31874	MO		78.870	76.489
alu1_198	20	44	4436	1.52674	57.004	3.195	19.726
c2_181	35	151	85613	MO		315.079	149.811
C7552_205	21	85	11143	MO		9.944	20.234
cm150a_210	22	74	547	MO		0.282	14.483
cm151a_211	28	52	8528	5.34664	62.886	7.246	20.718
cm163a_213	29	55	2891	error		1.972	23.421
dk27_225	18	33	5550	1.005	56.381	2.339	17.351
example2_231	16	167	14976	MO		17.405	22.143
mlp4_245	16	139	16500	MO		22.521	20.107
d5adder_306	32	102	78068	MO		212.609	45.793
rd84_313	34	112	73617	MO		206.177	80.945
sym9_317	27	71	52742	MO		107.998	43.827

its noisy implementation modeled by a superoperator in the form of a set of $2^n \times 2^n$ matrices $\mathcal{E} = \{E_i\}$ is calculated by

$$F_J(\mathcal{E}, U) = \frac{1}{2^{2n}} \sum_i |\operatorname{tr}\left(U^\dagger E_i\right)|^2. \tag{10}$$

Based on Eq. (10), Alg. I in [7] computes $\operatorname{tr}\left(U^\dagger E_i\right)$ for each E_i individually and the cardinality $|\mathcal{E}|$ of $\mathcal{E}$ grows exponentially in the number of noisy gates in a circuit. By rewriting F_J as

$$F_J(\mathcal{E}, U) = \frac{1}{2^{2n}} \sum_i |\operatorname{tr}\left(U^\dagger E_i\right)|^2 = \frac{1}{2^{2n}} tr((U^\dagger \otimes U^T)M_{\mathcal{E}}), \tag{11}$$

for $M_{\mathcal{E}} = \sum_i E_i \otimes E_i^*$. Alg. II in [7] improves Alg. I and calculates $\sum_i |\operatorname{tr}\left(U^\dagger E_i\right)|^2$ collectively by contracting a single tensor network. However, the matrix size in Eq. (11) becomes $2^{2n} \times 2^{2n}$.

Table 5: Results on noisy BV benchmarks.

#Q	TDD Alg. II		SliQEC							
			#Trials = 10^1		#Trials = 10^2		#Trials = 10^3		#Trials = 10^4	
	Time	F	Time	F	Time	F	Time	F	Time	F
10	0.304	0.9714	0.023	0.9000	0.219	0.9800	2.190	0.9710	21.822	0.9724
20	0.735	0.9427	0.061	0.9000	0.574	0.9700	6.071	0.9340	60.574	0.9418
30	1.571	0.9149	0.135	0.9000	1.432	0.9500	15.094	0.9280	152.511	0.9169
40	2.309	0.8878	0.437	0.7000	2.698	0.9300	28.930	0.8850	296.599	0.8828
50	3.270	0.8616	0.578	0.8000	5.561	0.8400	51.812	0.8660	542.772	0.8572
60	7.229	0.8361	1.153	0.9000	8.719	0.9100	83.460	0.8410	684.991	0.8389
70	6.698	0.8114	1.319	0.7000	12.152	0.8700	125.983	0.7990	1070.360	0.8105
80	8.475	0.7874	1.822	0.9000	17.249	0.7800	176.257	0.7960	1454.800	0.7843
90	10.539	0.7641	2.482	1.0000	26.806	0.8100	288.594	0.7600	1978.120	0.7699
100	12.588	0.7415	3.338	0.9000	38.689	0.7400	339.547	0.7300	2474.870	0.7436
700	MO		25.358×10^1		25.358×10^2		25.358×10^3		25.358×10^4	
800	MO		37.476×10^1		37.476×10^2		37.476×10^3		37.476×10^4	
900	MO		44.095×10^1		44.095×10^2		44.095×10^3		44.095×10^4	

Note that for each E_i in Eq. (10), $|\operatorname{tr}\left(U^\dagger E_i\right)|^2$ is similar to Eq. (8), and thus can be calculated by our method when E_i is algebraically representable. Using Monte Carlo simulation [9], the real probability distribution given a set of noisy gates can be approximated by simulating a large number of trials with noisy gates being injected into an ideal circuit according to the error probabilities. We conducted experiments to study the applicability of our methods to equivalence checking of noisy circuits by the following setting.

We took BV benchmarks as the ideal U circuits. For the noisy implementation, every gate in U is followed by an depolarizing channel $N(\rho) = p\rho + \frac{1-p}{3}(X\rho X + Y\rho Y + Z\rho Z)$ [10], where ρ is a density matrix describing a mixed state, p is the error probability setting to 0.001 in the experiments. The results are shown in Table 5, where Alg. I results were not reported because it timed out on all the cases. It should be noted that because Alg. II and SliQEC were implemented in python and C++, respectively, their runtimes cannot be directly compared. From Table 5, we see that the fidelity computed by SliQEC well approximates that of Alg. II with 1000 to 10000 trials. Although Alg. II was advantageous in computing fidelity for small qubit circuits, it suffers from the memory explosion problem for circuits with more than 700 qubits. In contrast, SliQEC exhibited superior scalability (runtime extrapolated for $\#Q \geq 700$) and can be parallelized for acceleration.

5.3 Sparsity Checking

In the experiment, the sparsity checking algorithms for QMDD and BDD discussed in Section 4.3 were implemented. The evaluation was performed on Random benchmarks, where circuits U are generated in the same way as in Section 5.1 except for the ratio of the number of gates to the number of qubits being set to 3:1. The results are shown in Table 6, where the DD build time and the sparsity computing time are reported. The results suggest the better scalability of the BDD-based method than the QMDD counterpart.

6 CONCLUSIONS

This paper has developed the bit-sliced BDD-based method for unitary matrix representation and manipulation. Its applications to equivalence checking, fidelity checking, and sparsity checking have been presented. Experiments have been conducted and demonstrated the superiority of the proposed approach to the state-of-the-art methods in scalability and accuracy. For future work, we would like to support checking for more quantum circuit properties.

Table 6: Sparsity checking on Random benchmarks.

#Q	#G	QMDD based			BDD based		
		Build time	Check time	TO/MO	Build time	Check time	TO/MO
20	60	0.181	0.003	0/0	0.502	0.004	0/0
25	75	13.296	0.296	0/0	2.944	0.023	0/0
30	90	121.793	0.579	0/0	8.952	0.042	0/0
35	105	585.719	2.286	3/0	22.848	0.182	0/0
40	120	1050.418	1.698	4/2	211.775	0.583	1/0
45	135	-	-	8/2	697.819	1.439	0/0
50	150	-	-	8/2	3282.897	2.896	7/0
55	165	-	-	8/2	2123.429	2.351	4/0
60	180	-	-	8/2	1590.066	1.244	8/0
65	195	-	-	8/2	2073.895	3.932	8/0

ACKNOWLEDGMENTS

This work was supported in part by the Ministry of Science and Technology of Taiwan under grants MOST 110-2224-E-002-011 and MOST 111-2119-M-002-012.

REFERENCES

[1] Héctor Abraham et al. 2019. *Qiskit: An Open-source Framework for Quantum Computing*. https://doi.org/10.5281/zenodo.2573505
[2] Antonio Acín, E. Jané, and Guifré Vidal. 2001. Optimal estimation of quantum dynamics. *Physical Review A* 64 (2001), 050302.
[3] Lukas Burgholzer and Robert Wille. 2021. Advanced Equivalence Checking for Quantum Circuits. *IEEE Transactions on Computer-Aided Design of Integrated Circuits and Systems* 40, 9 (2021), 1810–1824.
[4] Cirq Developers. 2021. *Cirq*. https://doi.org/10.5281/zenodo.5182845
[5] Alexei Gilchrist, Nathan K. Langford, and Michael A. Nielsen. 2005. Distance measures to compare real and ideal quantum processes. *Physical Review A* 71, 6 (2005).
[6] Aram W. Harrow, Avinatan Hassidim, and Seth Lloyd. 2009. Quantum Algorithm for Linear Systems of Equations. *Physical Review Letters* 103, 15 (2009).
[7] Xin Hong, Mingsheng Ying, Yuan Feng, Xiangzhen Zhou, and Sanjiang Li. 2021. Approximate Equivalence Checking of Noisy Quantum Circuits. In *Proc. DAC*. 637–642.
[8] Xin Hong, Xiangzhen Zhou, Sanjiang Li, Yuan Feng, and Mingsheng Ying. 2020. A Tensor Network based Decision Diagram for Representation of Quantum Circuits. *CoRR* abs/2009.02618 (2020).
[9] Gushu Li, Yufei Ding, and Yuan Xie. 2019. SANQ: A Simulation Framework for Architecting Noisy Intermediate-Scale Quantum Computing System.
[10] Michael A. Nielsen and Isaac L. Chuang. 2000. *Quantum Computation and Quantum Information.*
[11] Philipp Niemann, Robert Wille, David Michael Miller, Mitchell A. Thornton, and Rolf Drechsler. 2016. QMDDs: Efficient Quantum Function Representation and Manipulation. *IEEE Transactions on Computer-Aided Design of Integrated Circuits and Systems* 35, 1 (2016), 86–99.
[12] Aditya K. Prasad, Vivek V. Shende, Igor L. Markov, John P. Hayes, and Ketan N. Patel. 2006. Data structures and algorithms for simplifying reversible circuits. *J. Emerg. Technol. Comput. Syst.* 2, 4 (2006), 277–293.
[13] Fabio Somenzi. 2005. CUDD: CU Decision Diagram Package (release 2.4.2). *University of Colorado at Boulder* (2005).
[14] Yuan-Hung Tsai, Jie-Hong R. Jiang, and Chiao-Shan Jhang. 2021. Bit-Slicing the Hilbert Space: Scaling Up Accurate Quantum Circuit Simulation. In *Proc. DAC*. 439–444.
[15] Robert Wille, Daniel Große, Lisa Teuber, Gerhard W. Dueck, and Rolf Drechsler. 2008. RevLib: An Online Resource for Reversible Functions and Reversible Circuits. In *Proc. ISMVL*. 220–225.
[16] Robert Wille, Nils Przigoda, and Rolf Drechsler. 2013. A compact and efficient SAT encoding for quantum circuits. In *Proc. Africon*. 1–6.
[17] Shigeru Yamashita and Igor L. Markov. 2010. Fast Equivalence-Checking For Quantum Circuits. In *Proc. NANOARCH*. 23–28.
[18] Alwin Zulehner, Stefan Hillmich, and Robert Wille. 2019. How to Efficiently Handle Complex Values? Implementing Decision Diagrams for Quantum Computing. In *Proc. ICCAD*. 1–7.
[19] Alwin Zulehner, Philipp Niemann, Rolf Drechsler, and Robert Wille. 2019. Accuracy and Compactness in Decision Diagrams for Quantum Computation. In *Proc. DATE*. 280–283.